Journal of Materials Chemistry A

Accepted Manuscript

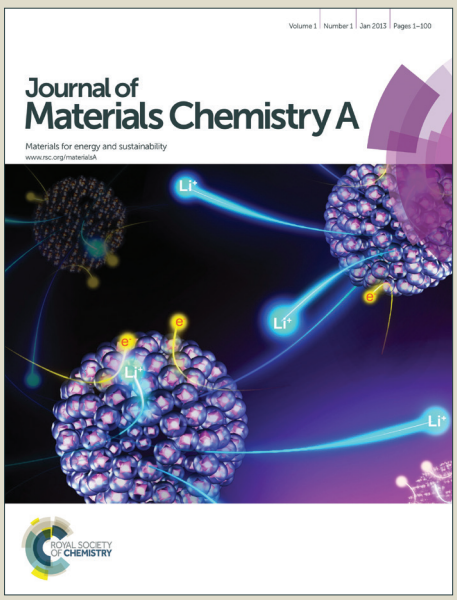

ROYAL SOCIETY OF CHEMISTRY

www.rsc.org/materialsA

Polymer Functionalization to Enhance Interface Quality of Mixed Matrix Membranes for High CO_2/CH_4 Gas Separation

Submitted to Journal of Materials Chemistry A

Nguyen Tien-Binh, Hoang Vinh-Thang, Xiao Yuan Chen, Denis Rodrigue and Serge Kaliaguine*

Department of Chemical Engineering, Université Laval, Canada, G1V 0A6

*Corresponding author: Serge Kaliaguine

Email: Serge.kaliaguine@gch.ulaval.ca, Tel.: 1 418 656 2708; fax: 1 418 656 3810

Abstract

Hydroxyl-functionalized homo- and co-polyimides 6FDA-$(DAM)_x$-$(HAB)_y$ (with x:y molar ratio of 1:0; 2:1; 1:1; 1:2) and two metal organic frameworks (MOFs), MIL-53(Al) and NH_2-MIL-53(Al) were synthesized for preparation of mixed matrix membranes (MMMs). The MOF loadings were varied over the range of 10-20 wt% for NH_2-MIL-53(Al) and 10-15 wt% for MIL-53(Al). The incorporation of hydroxyl groups into the polyimide backbone is expected to improve the interfacial interaction between the polymer matrix and fillers, consequently, enhancing gas separation performance of MMMs. A big increase in glass transition temperature (T_g) for MMMs confirmed the polymer chain rigidification, which was caused by a strong interaction between the hydroxyl groups in the copolyimides and the amine groups in NH_2-MIL-53(Al). Additionally, SEM results showed that the hydroxyl groups facilitated the particle dispersion in the MMMs, either was NH_2-MIL-53(Al) or MIL-53 used as filler. Gas separation performances of MMMs were characterized by both CO_2/CH_4 pure gas and binary permeation measurements at 35 °C and 150 psi. The incorporation of NH_2-MIL-53(Al) in the hydroxyl-copolyimides was found to significantly improved the CO_2/CH_4 separation factor while maintaining CO_2 permeability of the MMMs as high as those of the neat corresponding copolyimides, therefore greatly enhancing the MMM separation performance. For example, the MMM prepared from 6FDA-DAM-HAB (1:1) copolyimide and 10 wt% NH_2-MIL-53(Al) showed a permeability/selectivity behavior approaching the 2008 Roberson's upper bound making it attractive for practical usage. The significant improvement in

CO_2/CH_4 separation factor observed for the MMMs made of the hydroxyl-copolyimides and the amine-functionalized MOFs was due to (i) the enhanced polymer-filler compatibility originated from a mutual interaction between the polymer-functional moieties and the amine-functionalized MOF surface yielding defect-free MMMs and (ii) the high CO_2/CH_4 selective adsorption in the NH_2-MIL-53(Al) framework.

Keywords: CO_2/CH_4 separation, mixed matrix membranes, hydroxyl-functionalized copolyimides, biogas separation, NH_2-MIL-53(Al).

1. Introduction

Polymer membrane-based gas separation has emerged as a competitive technology for conventional ones such as distillation and absorption based processes, which demand high energy consumption for a phase change to separate gases. Membrane separation technology, on the other hand, does not require a phase change thus saving operational cost [1]. Furthermore, it has relatively smaller footprints than other methods because no distillation or stripping column is employed [2]. Gas separation through membranes is fundamentally based on molecular differences in size and shape and interaction with membranes [3].

Polymer membranes have been used in many gas separation plants for natural gas purification (CO_2 removal before sending bio-methane to the pipeline), hydrogen isolation and recovery, nitrogen production or oxygen enrichment from air [4]. Additionally, thanks to the eases of operation, there is a rapid growth in application of membrane-based separation for purifying landfill gas and biogas, which are often produced in facilities located in the countryside [5].

Gas separation performance of a membrane is mainly evaluated by its *selectivity* and *permeability*. Generally, membranes possessing both high selectivity and permeability are utmost desirable since they are able to achieve a given capacity at lower driving force and smaller membrane area separation. Current applications based on membrane separation include oxygen and nitrogen air enrichment, hydrogen recovery, natural gas separation and VOCs (volatile organic compounds) removal from effluent wastes,…[6]. Criteria for selecting material for each separation might be variable, for example, according to Merkel et al. [7] a membrane with very high permeability and good selectivity may be more attractive for CO_2 capture in power plant post-combustion.

For polymer membranes, however, a well-known trade-off relation between permeability and selectivity was reported by Robeson: the so-called Roberson's upper bounds [8-10]. Neat polymer membranes can approach but rarely surpass the upper bound limit. Modifying a polymer with inorganic fillers such as zeolites, mesoporous silicas, activated carbons, carbon nanotubes and metal-organic frameworks (MOFs), forming mixed matrix membranes (MMMs), is a potential method to boost performance [11, 12]. Among

those, the MOFs offer obvious advantages including a relatively higher separation performance owing to their size/shape exclusion or selective adsorption properties and better compatibility with the polymer phase. The pore size and chemical properties of MOFs can be tuned easily by means of organic linker substitution.

The interphase quality in MMMs is one of the most important factors determining the gas selectivity of membranes. The most frequent defective morphology is the formation of voids at the polymer-filler interface in MMMs using inorganic fillers, such as zeolites. The interface voids will create new bypasses around the fillers for gas transport within the MMMs, therefore, deteriorating the membrane separation properties. Using MOFs as filler is expected to eliminate those voids because the presence of organic linkers, intrinsic in the MOF structure, make their surface more carbophilic leading to a better affinity and compatibility with polymers. However, an insufficient adhesion between fillers and polymer has been detected for many MOF-based MMMs [13, 14], accompanied with defective interfaces and even leading to lower selectivities of the MMMs than the neat polymers. A strategy to create a better contact at the polymer-MOF interface has been developed for MMMs adopting zeolitic imidazolate frameworks (ZIFs) with nano-sized particles as fillers [15-18]. Permeabilities of those MMMs were found to be significantly increased for all the tested gases (O_2, N_2, CO_2, CH_4, C_3H_6, C_3H_8), however the CO_2/CH_4 selectivity was either unchanged or decreased upon increasing ZIF loading. The interface voids between the nano fillers and polymers, although undetectable in SEM micrographs because of their nano scales, are supposed to be the main reason for the poorer selectivity. Another approach to improve the polymer-MOF adhesion is to modify the MOF external surface with functional groups, which can make hydrogen bonding with functional groups of the polymer chains. Zornoza *et al*. prepared NH_2-MIL-53(Al)/polysulfone MMMs which showed two times increase in CO_2/CH_4 ideal selectivity without sacrificing CO_2 permeability at 25 wt% loading [19]. The enhanced permselectivity was attributed to the CO_2/CH_4 selective adsorption of NH_2-MIL-53(Al) and the good polymer-MOF adhesion induced by hydrogen bonding between the amine and sulfone groups. However, the MMM performance was far below the Robeson's upper bound due to a slow gas permeation across polysulfone, about 3 Barrer for CO_2, that could not be compensated by the

filler. Recently, Seoane *et al.* used two sulfur-containing copolyimides as the continuous phase and amino functionalized MOFs as dispersed phase to investigate the effect of polymer functionality on the resulting MMMs separation properties [20]. It was found that, at 10 wt.% loading of NH_2-MIL-101(Al), the polymer comprising $–SO_2$ sulfone groups showed better affinity with the fillers than its counterpart having –S sulfide ones, hence, its performance was improved approaching the Robeson 1991 H_2/CH_4 and CO_2/CH_4 upper bound limits. These improvements were attributed to the flexibility, porosity of filler and sulfone functional groups, as well as polymer rigidification.

In order to elucidate the contribution of functional groups in MOF to MMM's gas separation, our group has intensively examined different polymers including Matrimid®, Ultem® and 6FDA (4,4'-hexafluoroisopropylidene diphthalic anhydride)-based polyimides for MMMs filled with various amine-functionalized MOFs such as NH_2-UiO-66, NH_2-MOF-199 [21] and NH_2-MIL-53 [22, 23]. In general, those MMMs delivered attractive performance with a steady increase in CO_2/CH_4 selectivity and minor loss in CO_2 permeability, therefore, shifting their performance upward and surpassing the 1991 Robeson's upper bound. However, the employed polymer was 6FDA-ODA (ODA = 4,4'-oxidianiline), a non-functional polyimide with very low gas permeation, for example less than 15 Barrer for CO_2 permeability [23], making the resultant MMMs unattractive for practical usage. Furthermore, a noticeable particle agglomeration and a weak polymer-MOF adhesion were detected in all the MMMs. This behavior of the amine-functionalized MOFs has raised the concern that polymer-MOF adhesion might be insufficient to compete with the MOF-MOF interaction, and therefore the particles were more likely to agglomerate forming clusters rather than being dispersed homogeneously in the bulk polymer.

In order to overcome those limitations, this study proposes an application of polymers grafted with functional groups as continuous phase combined with amine-functionalized MOFs as dispersed phase for MMMs. The introduction of some functional groups in the polymer chains is expected to enhance polymer-MOF interaction owing to hydrogen bonding between amine groups in the filler and those functional groups, thereby the MOF particle spatial distribution will be improved. Moreover, not only these functional groups but also the polymer intrinsic permeability is of great important to control the

overall performance of obtained MMMs. To do so, a range of copolyimides containing both bulky structure and hydroxyl groups derived from two diamines, namely 2,4-diaminomesitylene (DAM) and a hydroxyl-inherent diamine, 3,3′-dihydroxyl-4,4′-diaminobipheny (HAB), respectively, were prepared. The diamine molar ratios of DAM to HAB were varied to control the hydroxyl group content in copolymers that is a key factor to fine-tune the polymer-filler affinity as well as permeability, so that filler particles could be embedded firmly but not blocked by the copolymers. The aim of this work is to study the correlation between the polymer-filler interaction and the MMM's gas separation performance, therefore, unmodified MIL-53(Al) and amine functionalized NH_2-MIL-53(Al) are employed as fillers for comparison.

2. Experimental

2.1. Materials

For the synthesis of homo- and co-polyimides, 4-4'-(hexafluoroisopropylidene)diphthalic anhydride (6FDA, >99%) and 3,3'-dihydroxy-4,4'-diamino-biphenyl (HAB, >99%) were obtained from Chriskey Co. and 2,4-diaminomesitylene (DAM, purified by vacuum sublimation) was supplied by Sigma Aldrich. 1-Methyl-2-pyrrolidone (NMP, anhydrous, 99.5%) and pyridine (ACS reagent, >99%) were purchased from Alfa Aesar and Sigma Aldrich, respectively.

For the synthesis of non- and amino-functionalized aluminum MIL-53, aluminum nitrate nonahydrate $Al(NO_3)_3.9H_2O$ (ACS reagent, >98%), 2-aminoterephthalic acid (> 99%) and terephthalic acid (> 99%) were ordered from Sigma Aldrich. Dimethylformamide DMF (99.8%) as solvent was also obtained from Sigma Aldrich. All the reagents were used as received.

2.2. MOF and polyimide syntheses

Non- and amino-functionalized aluminum MIL-53 (denoted MIL-53 and NH_2-MIL-53, respectively) were synthesized by a method as described in our previous work [23]. First, terephthalic acid (for MIL-53) or 2-aminoterephthalic acid (for NH_2-MIL-53) was mixed with aluminum nitrate nonanhydrate in DMF at molar ratio of $Al(NO_3)_3$: terephthalic acid (or 2-aminoterephthalic acid) : DMF = 1:1.48:184.5. The obtained solution was then aged at room temperature and transferred to a Teflon-lined steel autoclave. The autoclave was kept in an oven for 3 days at 130 °C. The obtained mixture was decanted after centrifugation at 5000 rpm for 15 min and collected as a product powder. To extract unreacted acid, the as-synthesized powder was washed twice with DMF in an autoclave at 130 °C for 24 h. DMF was removed by acetone Soxhlet extraction for 20 h. Finally, the white (MIL-53) or yellow (NH_2-MIL-53) colored product was dried at 200 °C in a vacuum oven for 48 h and stored in a vacuum desiccator.

6FDA-DAM (denoted FD) homo-polyimide was synthesized by a two-step polycondensation as published previously [21]. In the first step, polyamic acid (PAA) derived from an equimolar mixture of dianhydride 6FDA and diamine DAM was prepared by solution condensation in anhydrous NMP. The mixture was mechanically stirred for 24 h under an argon atmosphere in a three-neck flask. The flask was then immersed in an ice-bath. In the second step, PAA was converted to polyimide by chemical imizidation. To the PAA solution, extra amounts of acetic anhydride (dehydrating agent) and pyridine (catalyst) were added. The mixture was stirred at room temperature under an argon atmosphere for another 24 h. The obtained liquid was precipitated in methanol, yielding a white powder FD polyimide. The obtained polyimide was washed several times with methanol before drying in a vacuum oven at 200 °C for 24 h.

6FDA-$(DAM)_x$-$(HAB)_y$ copolyimides (denoted FDH-xy) (Fig. 1) were prepared by a similar procedure. In the first step, three PAAs were obtained from equimolar blend of 6FDA and mixed diamines (molar ratio DAM:HAB = 2:1 or 1:1 or 1:2). In the second step, no dehydration agent was employed to avoid esterification of hydroxyl functional groups in HAB moiety. To the PAA solution, pyridine and toluene

were added (volume ratio of pyridine: toluene = 1:4) and the mixture was then heated to 160 °C under an argon atmosphere. During imizidation, water was removed using a Dean-Stark trap. Upon repeated precipitation in methanol/water (v:v = 1:1) and drying in a vacuum oven at 120 °C for 24 h, light-yellow copolyimide powders were collected. In this work, the copolyimides were denoted according to the molar ratio of diamines as indicated in Table 1.

Fig. 1

Table 1

2.3. Preparation of mixed matrix membranes

0.5 g of polymer was dissolved in 15 ml of THF solvent (5 wt%) to form a polymer solution, which was further filtered using a 1.0 μm filter. An amount of NH_2-MIL-53 (or MIL-53), defined by Eqn.(1) corresponding to the MOF loading, was dispersed in 5 ml of THF, followed by a strong sonication to get MOF slurry.

$$MOF\ loading\ (wt\%) = \left(\frac{MOF\ wt}{MOF\ wt + Polyimide\ wt} \right) \times 100\% \quad (1)$$

A so-called "priming" technique was applied in MMMs preparation to promote filler distribution in the polymer matrix, as well as to prevent void formation [24]. About 10 wt% of the polymer solution was first introduced into the whole MOF slurry. The resulting mixture was magnetically stirred for 2 hours before the rest of the polymer solution was added. The solution was further stirred until the remaining volume was 3-5 ml upon THF evaporation. Before casting on a glass plate restrained by a metal ring, the solution was sonicated for 3 min to avoid particle agglomeration. Thereafter, the remained THF solvent was evaporated at room temperature for 24 h. The nascent membrane was removed carefully from the glass plate by soaking in water and drying in a vacuum oven for 24 h at 120 °C. Finally, the membranes were kept in a vacuum desiccator.

2.4. Pure-gas permeation measurements

Pure-gas permeation coefficients of all membranes were determined using the constant volume/variable pressure method. Once the membrane was placed securely in a permeation cell, both the feed and permeate sides were evacuated for 5 hours. A pure gas was then charged to the feed side and pressurized at 150 psi while the permeated gas at the other side of membrane was collected into a closed-chamber, where the data of pressure change was recorded as a function of time using an electronic transducer. The order of gas permeation measurement was methane and then carbon dioxide. The experimental temperature was constant at 35 °C.

The steady flux, J, determined by the constant volume/variable pressure method, can be calculated as:

$$J = \frac{22414}{A}\frac{V}{RT}\frac{dp}{dt} \tag{2}$$

where J is the steady-state flux (cm^3 (STP) cm^{-2} s^{-1}), A is the membrane area (cm^2), V is the constant volume of the closed chamber (cm^3), R is the universal gas constant (6236.56 cm^3cmHg mol^{-1} K^{-1}), T is the absolute temperature (K) and dp/dt is the rate of pressure increase in the closed chamber at steady flux (cmHg s^{-1}). The gas permeation coefficient P (cm^3(STP) cm cm^{-2} s^{-1} $cmHg^{-1}$) is given by the following expression:

$$P = \frac{Jl}{(p_2 - p_1)} \tag{3}$$

where l is the membrane thickness (cm), while p_2, p_1 are the feed pressure and permeate pressure (psi), respectively. Pure-gas selectivity, α, is calculated as the ratio of permeation coefficients of gases A and B using Eqn.(4). A is usually ascribed to the higher permeation gas.

$$\alpha_{AB} = \frac{P_A}{P_B} \tag{4}$$

2.5. Mixed-gas permeation measurement

Mixed gas permeation measurements were conducted using the same protocol as for the pure-gas, except that the feed side was charged with a CO_2/CH_4 gas mixture (v:v = 50:50) at a pressure of 150 psi and 35 °C. The mixed-gas permeability coefficients for each gas component, for example *A*, can be determined as [25]:

$$P_A = \frac{y_A J_{perm} l}{(p_{feed} x_A) - (p_{perm} y_A)} \quad (5)$$

where y_A and x_A are the mole fractions of component *A*, determined by means of a gas chromatograph equipped with a thermal conductivity detector, in the permeate and feed side, respectively. J_{perm} is total permeate flux of the gas mixture determined by Eqn. 2 ($cm^3\ cm^{-2}\ s^{-1}$), l is the membrane thickness (cm), p_{perm}, p_{feed} are the permeate pressure and feed pressure (cmHg), respectively. The mixed-gas selectivity, or so-called separation factor, can be estimated as:

$$\alpha^*_{AB} = \frac{(y_A / y_B)}{(x_A / x_B)} \quad (6)$$

where y_A, y_B and x_A, x_B are the mole fractions of components *A* and *B* in the permeate and feed side, respectively.

The diffusion coefficient (*D*) is estimated by the time-lag method [26] as:

$$D = \frac{l^2}{6\theta} \quad (7)$$

where θ is the time-lag (s), *l* is the membrane thickness (cm). The solubility coefficient (*S*) is estimated from the pure-gas permeability coefficient (*P)* and the diffusion coefficient (*D*) by the following equation:

$$P = DS \quad (8)$$

3. Characterization

Glass transition temperatures (T_g) of the MMMs were determined using a dynamic mechanical thermal analyzer (TA Instruments, RSA-3, New Castle, DE) on sample films with a dimension of 20×6×0.05 mm^3. The temperature was ramped from 30 to 500 °C at a rate of 3 °C/min at a strain of 0.05 % and a frequency of 1 Hz. To determine *T*g, three samples of each membrane were taken for measurement. FTIR spectra analysis was conducted using a Nicolet Magna 850 Fourier transform infrared spectrometer (Thermo Scientific, Madison, WI) equipped with a liquid-nitrogen-cooled narrow-band MCT detector and Golden-Gate (diamond IRE) ATR accessories (Specac Ltd., London, U.K.). Each spectrum was obtained from the acquisition of 128 scans at 4 cm^{-1} resolution from 4000 to 700 cm^{-1} using Happ−Genzel apodization. Particle size and particle size distribution were measured from suspensions on a Zetasizer Nano ZS. Scanning electron micrographs (SEM) were employed to characterize both crystal size of the dispersed phase and morphology of the membranes using a JEOL JSM-840A operated at 15-20 kV. Nitrogen adsorption isotherms were measured at -196°C to characterize the textural properties of the MOF particles, including the total BET surface specific area and micropore volume (Nova 2000, Quantachrome Corp., USA). Powder X-ray diffraction patterns (XRD) were recorded using a Siemens D5000 powder diffractometer with Cu Kα radiation (λ = 1.5406 Å).

4. Results and discussion

4.1. Characterization of MOFs

Scanning electron micrograph images of the MIL-53 and NH_2-MIL-53 crystals are shown in Fig. 2. The diameter of MOF particles was estimated to be in the range of 100-200 nm, and there was no difference in morphology between the modified and unmodified MOFs. Particle size and particle size distribution were further measured by dynamic light scattering (DLS) indicating a maximum in the size range of 100-190 nm for NH_2-MIL-53 and in the size range of 190-340 nm for MIL-53 (Fig. 3).

Table 2 presents the physical properties of the unmodified MIL-53 and amino-functionalized NH_2-MIL-53. The functionalized MIL-53 displays a smaller micropore volume than that of the unmodified because of the presence of functional groups inside the one-dimensional channels [27]. In addition, the lower specific surface specific area and higher density are related to hydrogen bonding between NH_2 groups and $[AlO_6]_\infty$ units since it stabilizes the narrow-pore structure of NH_2-MIL-53 [28, 29].

Fig. 4 shows FTIR spectra for MIL-53 and NH_2-MIL-53 powder over the wavenumber range of 750-4000 cm^{-1}. The main bands related to the inherent amino groups in the linker are 1629 cm^{-1} δ (NH_2), 1340 and 1257 cm^{-1} ν(C_{ar}–N). Additionally, the two bands at 3390 and 3502 cm^{-1} in the spectrum of NH_2-MIL-53 refer to the symmetric and asymmetric vibration of –NH_2 groups, respectively.

Fig. 2

Fig. 3

Table 2

Fig. 4

4.2. Characterization of MMMs

Density and glass transition temperatures (T_g) of the homo- and co-polymer precursors and their MMMs are provided in Table 3. The measured density of FD and copolymers are compatible with those reported previously [30, 31]. The homo-polymer FD possesses the lowest density value due to a bulky structure of the DAM moiety, which inhibits packing efficiency of polymer chains. When DAM is partially substituted by HAB in the copolymers, hydroxyl groups in HAB enhance the chain-chain interaction, leading to higher copolymer density. For MMMs, increasing density with increasing MOF loading was observed. The main reason is that MOF particles decrease inter-chain spacing of the polymers, resulting from a good affinity between MOFs and polymers. In consequence, the polymer layer around MOF particles becomes denser and has higher density than the bulk polymer. Such density increase of MMMs upon ZIF-90 introduction was reported in the literature [32]. Introduction of MOF particles also induced higher T_g values for MMMs compared with the corresponding polymers. In our case, this increase is more significant for hydroxyl

containing copolyimides than for non-hydroxyl polyimide FD. As an example, for MMMs having 10 wt% NH_2-MIL-53, T_g increased by 11 °C for FD membrane, while a 21 °C increase was observed for FDH-11. This confirms that hydroxyl-copolyimides show stronger chemical affinity with amine-functionalized MOFs than the non-hydroxyl polyimide. This affinity is attributed to hydrogen bonding between hydroxyl groups of HAB moiety and the amine groups of amine-functionalized particles, additionally, the more flexible polymer backbone due to the HAB incorporation could also facilitate a better filler-polymer contact [20]. Obviously T_g rises due to polymer chain rigidification induced by MOF addition. Nevertheless, when MOF loading was higher than 10 wt%, T_g started decreasing because of the particle sedimentation and agglomeration, which happened more seriously at higher loadings (as seen Fig. 8C). Variation in T_g with MOF loading was also reported in the literature. Hsieh *et al.* observed a 5 °C increase in T_g related to Matrimid® composite filled with MIL-53 [14]. MMMs based on Matrimid® and benzylamine-modified C_{60} showed a 14 °C increase in T_g, owing to a strong affinity between Matrimid® and modified C_{60} [33]. This behavior was also observed for zeolite A/polyether-sulfone [34] and silica/polyimide [35] MMMs. A 14 °C T_g increase for calcined mesoporous ZSM-5/Matrimid® membrane was reported by Zhang *et al.* compared to only a 1 °C increase in T_g when uncalcined mesoporous ZSM-5 was used. More important change in T_g was explained by polymer chain penetration into the mesopores of calcined ZSM-5 [36].

Table 3

XRD patterns of the NH_2-MIL-53 crystals and their MMMs with FDH-11 are shown in Fig. 6. For amine-functionalized MIL-53, the experimental XRD pattern shows two main characteristic peaks at 2-*theta* = 9.2 and 18.2° [37, 38] suggesting the simultaneous appearance of both the narrow-pore and large-pore forms. It is known that peak patterns of NH_2-MIL-53 change upon the guest molecules trapping inside the pores due to its breathing property. These peaks are also observed in the NH_2-MIL-53/FDH-11 MMMs, demonstrating that the MMM production procedure did not change the filler crystal structure. For unmodified MIL-53 sample, a strong characteristic peak at 2-*theta* = 8.7° and two weaker characteristic peaks at 2-*theta* = 15.0° and 17.5° are corresponding to the large pore framework of MIL-53 structure [14, 39] (Fig. 7). The XRD pattern of the 15 wt% MIL-53/FDH-11 membrane also shows a major characteristic

peak at 2-*theta* similar to that of MIL-53, indicating that the MOFs maintained their structure in the MMMs. Moreover, an interesting feature is that the MOF characteristic peaks in MMMs were slightly shifted toward higher 2-*theta* angle suggesting good filler-polymer adhesion and referring to some possible polymer chain penetration into the NH_2-MIL-53(Al) framework [40].

The good interaction induced by hydrogen bonding between the amine functionalized MOF and the copolyimides containing hydroxyl groups was further confirmed by FTIR spectra shown in Fig. 5, in which υ_s(N−H) of NH_2-MIL-53 slightly shifted from 3390 to 3388 cm^{-1} for 10 wt.% NH_2-MIL-53/FDH-11. Furthermore, it shifted more strongly to 3384 cm^{-1} for the 15 wt.% NH_2-MIL-53/FDH-12 sample, where the hydroxyl moieties in copolyimides and the MOF content were both increased. On the contrary, there was no shifted band related to the $–NH_2$ groups observed for MMMs fabricated from the non-hydroxyl polyimide, for example 10 wt% NH_2-MIL-53/FD. The υ_{as}(N−H) band at 3500 cm^{-1} was unchanged in all samples, suggesting the hydrogen bonding had less influence on the asymmetric vibration of $–NH_2$ groups.

Fig. 5

Fig. 6

Fig. 7

Cross-section micrographs of the hydroxyl-copolyimide FDH-11 based MMMs with different MOF loadings were taken to investigate the effect of filler dispersion within copolymer matrix as a function of their loading and nature. Excellent compatibility and good interfacial interaction between NH_2-MIL-53 and the hydroxyl-copolymer FDH-11 are observed in Fig. 8, which shows a homogenous distribution of MOF particles with a size of 200 nm, within the membranes. Particularly, at 10 wt% and 15 wt% NH_2-MIL-53 loadings, all the particles were well dispersed and fully covered by a polymer layer (Fig. 8A and B). However, when the MOF content was raised to 20 wt% (Fig. 8C), particle sedimentation occurred at the bottom of the membrane suggesting the polymer content was likely insufficient to hold all MOF particles discretely. Within the sedimentation layer, a good polymer-filler adhesion was maintained that was proven by the formation of “wire” or “bridge” morphology. A similar behavior was also observed for

MMMs prepared from other hydroxyl-copolyimides including FDH-12 and FDH-21. The good particle dispersion morphology was attributed to the hydrogen bonding between amine functional groups of the NH_2-MOFs and hydroxyl groups of the copolymer matrix. In contrast, Fig. 9 illustrates the crater-like morphology for a NH_2-MIL-53/FD membrane made of the non-hydroxyl polyimide, in which the NH_2-MOF particles agglomerated into clusters with diameter of ca. 500 nm and their bare surface could be observed easily. The absence of hydroxyl groups in polymer matrix corresponded to a lack of the polymer-MOF hydrogen bonding that was supposed by the main reason for the MOF aggregation. In this case, the MOF-MOF interaction, induced by $–NH_2$ groups, was overwhelming over the polymer-MOF adhesion. It could be concluded that the hydroxyl groups played a critical role in improving the interaction between the NH_2-MOF particles and the polymer matrix, thereby enhancing the particle dispersion as well as effectively eliminating the interface voids.

Fig. 8

Fig. 9

In order to confirm the above statement, a non-functional MIL-53 was dispersed in the hydroxyl copolyimide, FDH-11, for MMM preparation. Interestingly, the hydroxyl groups helped creating defective-free interface morphologies for all the MIL-53 based membranes. At 10 wt% MIL-53, all the particles were well embedded in the copolymer matrix without agglomeration, as can be seen in Fig. 10A. At a higher MOF loading of 15 wt% (Fig. 10B), the MOF/polymer interaction seemed to be weaker, the particles showed a tendency to emerge from the copolymer but the void-free interface morphologies were maintained. The hydroxyl-copolymer has efficiently prevented the MIL-53 particle agglomeration that had been observed for many MIL-53/MMMs using non-functionalized polyimides such as P84® [13] or Matrimid® [14, 41, 42]. It is plausible to believe that the –OH groups have interacted with $AlO_4(OH)_4$ nodes in MIL-53 frameworks yielding better polymer-MOF affinity, which is in agreement with the above XRD analysis.

Fig. 10

4.3. Mixed gas permeation: Influence of co-polyimides composition and MOF loading

The diamine molar ratio of DAM to HAB was varied discretely from 1:0 to 2:1; 1:1 and 1:2 corresponding to the increase in hydroxyl functionalization from 0.0 to 33.3; 50.0 and 66.6 mol%, respectively. Among the neat polymer membranes, the polyimide without hydroxyl groups, FD, showed the highest CO_2 permeability coefficient of 315 Barrer, but the lowest CO_2/CH_4 separation factor of 9.7 for the CO_2/CH_4 gas mixture (Fig. 11). The presence of a diamine DAM with three methyl groups connected to two *ortho* positions to each imide ring makes the polymer chain packing less efficient. This is responsible for the high permeability but low selectivity of the FD membrane [30]. When DAM was partly substituted for hydroxyl-containing diamine HAB, a clear improvement in separation performance of the co-polymers was observed. CO_2/CH_4 separation factor increased proportionally to the HAB:DAM molar ratio in copolyimides, being 21.3, 34.1, and 53.5 for FDH-21, FDH-11 and FDH-12, respectively. This is because of a gradual enhancement of interchain interaction induced by hydroxyl groups when the HAB:DAM molar ratio increased [43]. As can be seen in Fig. 11, the CO_2 permeability of the copolyimides decreased obviously with increasing HAB:DAM molar ratio. A further addition of diamine HAB into the copolymers would result in a very small CO_2 permeability, making them less attractive for gas separation. This was therefore not further investigated in this work. It was reported that CO_2 permeability of 6FDA-HAB membranes is in the 3.0-12.0 Barrer range [31, 44, 45].

NH_2-MIL-53 particles were dispersed at 10-20 wt% loadings in co-polyimides FDH to investigate the influence of hydrogen bonding, stimulated by $–NH_2$ groups in the MOF framework and –OH groups in the HAB moieties, on the MMM separation performances. The incorporation of NH_2-MIL-53 induced a slight reduction in CO_2 permeability and significant improvement in CO_2/CH_4 separation factor for MMMs compared to the neat polymer membranes. For example, at the same 10 wt% MOF loading, MMMs with non-hydroxyl polyimide FD and three hydroxyl-copolyimides FDH-21, FDH-11 and FDH-12 displayed improvements in separation factors of 50%, 200%, 220% and 160% respectively. The worse separation performance of non-hydroxyl MMM was due to the formation of filler clusters, as seen in Fig.

9, where vacancies located inside the clusters might act as non-selective pathways, therefore, decreasing the overall membrane selectivity. The better selectivities of the MMMs based on hydroxyl-copolyimides over their non-hydroxyl counterpart was attributed to the excellent particle distribution involving a chemical interaction between the filler particles and the copolyimides. This helps avoiding the formation of nano-voids, though invisible in SEM images, in adjacent areas surrounding the fillers, which often deteriorates the separation performance of MMMs. This strong affinity should furthermore result in "a rigidified polymer" layer at the filler-polymer interface explaining the slightly decreased CO_2 permeabilities. For the influence of NH_2-MIL-53 loading on gas separation, the noticeable decline in CO_2/CH_4 separation factor and the insignificant change in CO_2 permeability, observed for all the 15-20 wt% NH_2-MIL-53/FDH-11 MMMs, were in accord with the above discussed morphology. The filler sedimentation ruined the homogeneity of MMMs yielding some particle-accumulated domains, where the polymer content was insufficient to completely cover all the particles, creating non-selective channels. In that case, the CO_2/CH_4 selectivity was more vulnerable than CO_2 permeability because gas transports in the channels were likely driven by Knudsen diffusion law, in which their separation is inversely proportional to the ratio of square root of the gas molecular weights [46] (estimated for CO_2/CH_4 selectivity at as low as 0.6). For that reason, the best separation performances, in this work, were found for MMMs containing the optimum loadings of ca. 10-15 wt%.

Non-functionalized MIL-53, having similar morphology to NH_2-MIL-53, was incorporated with a hydroxyl copolyimide, FDH-11, for comparison. The resulting CO_2 permeabilities and CO_2/CH_4 separation factors are illustrated in Fig. 12. All the investigated MMMs show enhanced CO_2 permeabilities and CO_2/CH_4 separation factor with increasing MIL-53 loading compared to the neat polymer membranes, suggesting a good adhesion between the MOFs and the polymers. The polymer chain rigidification is thought responsible for the slight increase in CO_2/CH_4 separation factor, whereas, the enhanced CO_2 permeability with MOF loading is mainly due to the open-pore framework (8.5 Å-8.5 Å) of MIL-53 being larger than the kinetic diameters of both CO_2 (3.3 Å) and CH_4 (3.8 Å) [14, 41]. Compared to MMMs filled with NH_2-MIL-53, those containing the MIL-53 show a slightly higher CO_2

permeability, but a significantly lower CO_2/CH_4 separation factor, indicating that the interaction of hydroxyl groups in FDH-11 and MIL-53 was relatively weak, therefore reducing the extent of polymer rigidification as well as plasticization resistance.

Fig. 11

Fig. 12

4.4. Pure gas permeation: Gas diffusivity and solubility coefficients of MOF/PI MMMs

To compare with the mixed gas separation results, the pure-gas permeation of CO_2 and CH_4 were carried out to measure the CO_2/CH_4 permeability (P), diffusivity (D), solubility (S) and respective coefficient ratios for hydroxyl-copolyimide FDH-11 based MMMs (see Table 4). In the case of MIL-53 loaded MMMs, CO_2 permeability increased but CO_2/CH_4 ideal selectivity decreased upon the increase in filler loading compared to those of the neat FDH-11 membrane. The enhanced permeability was attributed to the large pore of MIL-53 that facilitated gas transports of both CO_2 and CH_4 because of the larger gas diffusivity within the porous fillers. However, gas permeations in the MIL-53 mainly follow the Knudsen diffusion law which makes CO_2 permeability is lower than CH_4, therefore, the ideal selectivity of MIL-53/MMMs was less than that of the neat polymer. For that reason, the diffusion selectivity (D_{CO_2}/D_{CH_4}) of the MMMs declined with increasing filler content.

On the contrary, the NH_2-MIL-53 addition induced a significant improvement in ideal selectivity for the MMMs. For example in this study, CO_2/CH_4 ideal selectivity of the 10 wt% NH_2-MIL-53/FDH-11 membrane was 4 times greater than that of the neat FDH-11. Such a high CO_2/CH_4 ideal selectivity was originating from the simultaneous increase in CO_2/CH_4 diffusivity selectivity and solubility selectivity of the MMMs. In those MMMs, the polymer-filler interaction was significantly improved due to the appearance of hydrogen bonding between the hydroxyl groups of copolyimide FDH-11 and amine groups in the filler. This might restrain free motions of some polymer segments including the hydroxyl groups and help the polymer packing become more efficient, therefore improving the diffusivity selectivity. Additionally, the NH_2-MIL-53 particles were capable of selectively adsorbing CO_2 over CH_4, over a wide

pressure range [29]. The presence of -NH_2 groups is more likely to increase the acidity of μ_2 –OH groups and more importantly to stabilize their framework flexibility, yielding a higher CO_2 adsorption selectivity, due to a specific interaction between CO_2 molecules and μ_2 –OH groups, similar to the non-functionalized MIL-53 [28]. In fact, the NH_2-MOF displays a zero-coverage adsorption enthalpy of 38.4 kJ/mol for CO_2, being significantly larger than that for CH_4 (ca. 20 kJ/mol). The CO_2/CH_4 solubility selectivity of the NH_2-MIL-53/MMMs was, therefore, greater than that of the neat polymer. This is because the solubility of a given gas in polymer membranes is decided by their free fraction volumes and their affinity to the gas molecule [2].

Data in Table 5 describing the permeability/selectivity behavior for some selected MMMs adopting the same MOF but different polymer matrix suggests that polymer selection is a key factor in MMMs performance. The hydroxyl-functionalized copolyimide FDH-11, in this work, had a good permeability-selectivity and was furthermore found to have high compatibility with the NH_2-MIL-53 filler, yielding MMMs possessing advanced separation performances.

Table 4

Table 5

4.5. Comparison with the Robeson's upper bound curves

Remarkably from our results, MMMs based on hydroxyl-functionalized copolymers with amine-functionalized MIL-53 showed outstanding performances in mixed gas separation. The separation performance in gas mixture (CO_2:CH_4 = 50:50) for selected membranes are compared with the Robeson's upper bounds in Fig. 13.

Overall, the combination of functionalized MOF, NH_2-MIL-53, and hydroxyl-functionalized copolymers produced new MMMs with outstanding gas separation performance. The MMMs showed a significant improvement in the CO_2/CH_4 separation factor and a minor loss in the CO_2 permeability, shifting their performance upward, surpassing the 1991 Robeson's upper bound. Interestingly, the 10 wt% NH_2-MIL-53/FDH-11 membrane was on the 2008 Robeson's upper bound. In contrast, the gas preparation data of

the MMMs using non-hydroxyl polyimide, FD, was somewhere far below the 1991 Robeson's curve. This highlighted the critical role of polymer polarity in the resulting MMM's performance. It is worth mentioning that gas separation of MMMs is strongly affected by nanoparticle morphology. The gas separation performance of a MMM is known to depend critically on the type of defective interface at the filler/polymer contact. The arrows in Fig. 13 corresponding to a steep increase in separation factor with loading is normally ascribe to a defective interface designated as "matrix rigidification" [11]. In this case, the thickness and permeability of the rigidified polymer layers determine the overall MMM gas separation [51]. In fact, no practical characterization allows measuring the interfacial thickness, but changes in T_g value of MMMs may confirm the presence of a rigidified layer [34, 52]. As can be seen in Table 3, T_g values of the MMMs with 10 wt% MOF loading were considerably higher than those of the neat polymers and decreased with increasing filler loading. This indicates that the value of 10 wt% was the optimal loading, at which, the rigidified layer might reach the thickest layer. Correspondingly, the separation performances of the MMMs with 10 wt% MOF loading were clearly better than the ones at 15-20 wt% MOF contents. On the other hand, gas permeability of the rigidified polymer layer is well known to depend on the filler-polymer affinity. In this work, the copolyimides were synthesized from diamine HAB including hydroxyl groups, which can interact with the amine groups of NH_2-MIL-53 by hydrogen bonding. Therefore, by increasing the molar ratio of HAB:DAM in copolyimides, one can increase the filler-polymer interaction. Fig. 13 shows that the CO_2/CH_4 separation factors of the MMMs containing 10 wt% NH_2-MIL-53 were improved at increasing HAB:DAM molar ratio, and reached a maximum value at a molar ratio of 1:1 before decreasing at a molar ratio of 2:1. This decrease may be explained by the partial pore blockage of MOFs interfering with the selective adsorption of CO_2 inside MOF particles.

Fig. 13

A different behavior was observed for MMMs containing unmodified MIL-53. The MIL-53 incorporation steadily improved CO_2 permeability and slightly modified CO_2/CH_4 separation factor of the MMMs (Fig. 14), and their separation performance could not surpass the 1991 Robeson's upper bound. This improvement was almost negligible for non-hydroxyl polyimide FD based MMMs and becoming more

pronounced for those made of the hydroxyl copolyimides. A perfectly horizontal arrow in Fig. 14 would correspond to an ideal non-defective interface. The small slope observed may therefore result from a thinner rigidified polymer layers around the MIL-53 particles compared to those of the NH_2-MIL-53 loaded MMMs. Additionally, the measured pure-gas diffusivity of CO_2 and CH_4 within the membranes comprising MIL-53, by the time-lag method, showed a marginal increase for both gases (see Table 4) indicating that the contribution of MIL-53 was to facilitate gas diffusion and the polymer rigidification was almost negligible. In MMMs, gas diffusion in the polymer phase is much slower than that in the fillers, therefore, the addition of fillers like MIL-53 can change gas diffusivity but hardly influence selectivity since it is mainly determined by the polymer phase which often accounts for more than 80 wt.% of MMMs. In case of NH_2-MIL-53 containing membranes, the filler possesses functional groups that can interact with –OH groups in the polymer backbones creating rigidified polymer layers on the filler surface, subsequently enhancing stiffness of the polymer chains. This implied that the introduction of NH_2-MIL-53 fillers not only improved the gas transport within MMMs, thanks to their porosity, but also affected the nature of polymer phase by restraining the flexibility of –OH diamine moieties. Another valuable contribution of the hydroxyl groups was to prevent the MIL-53 particle agglomeration and to produce homogeneous membranes without interface defects.

Fig. 14

This finding emphasizes that compatibility or affinity between the filler and polymer matrix is one of the main factors affecting MMM separation performance. Combining copolymers containing functional groups with amino-functionalized MOFs is an effective approach to solve the incompatibility problem.

5. Conclusion

A series of NH_2-MIL-53 loaded MMMs from three 6FDA based-copolyimides containing hydroxyl groups namely 6FDA-$(DAM)_x$-$(HAB)_y$ (x:y ratio =2:1; 1:1; 1:2) were prepared and compared with those from the non-hydroxyl polyimide 6FDA-DAM to systematically study how the polymer polarity and the

filler surface functionality affect the membrane selectivity-permeability property. It was found that the hydroxyl-copolyimides displayed a much better filler-compatibility behavior than their non-hydroxyl counterpart, which was attributed to hydroxyl bonding between the hydroxyl moieties of the copolyimides and the $–NH_2$ groups in the functionalized MOFs. This was further confirmed by the SEM analysis that showed excellent polymer-filler adhesion as well as particle dispersion in the hydroxyl-copolyimide based MMMs. Consequently, those MMMs exhibited much greater CO_2/CH_4 separation factor than that of the neat copolymers while maintaining good CO_2 permeability. The selectivity-permeability properties of all the NH_2-MIL-53/FDH MMMs have been compared with the Robeson's upper bounds, showing a promising prospect for industrial applications. Remarkably, 10 wt% NH_2-MIL-53/FDH-11 membrane is located on the 2008 Robeson's upper bound. The high CO_2/CH_4 separation performance is attributed to (i) the enhanced polymer-filler interaction as well as polymer chain rigidification induced by a strong interaction between amine- and hydroxyl-functionalized groups in MMMs, and (ii) the CO_2/CH_4 competitive adsorption inside the one-dimensional framework of NH_2-MIL-53.

6. Acknowledgements

The authors acknowledge the financial support of the Natural Sciences and Engineering Research Council of Canada (NSERC).

7. References

1. W. J. Koros, *AIChE J.*, 2004, 50, 2326-2334.
2. N. Du, H. B. Park, M. M. Dal-Cin and M. D. Guiver, *Energy Environ. Sci.*, 2012, 5, 7306-7322.
3. B. Zornoza, C. Tellez, J. Coronas, J. Gascon and F. Kapteijn, *Micropor. Mesopor. Mater.*, 2013, 166, 67-78.
4. W. J. Koros and R. Mahajan, *J. Membr. Sci.*, 2000, 175, 181-196.
5. S. Basu, A. L. Khan, A. Cano-Odena, C. Liu and I. F. Vankelecom, *Chem. Soc. Rev.*, 2010, 39, 750-768.

6. T.-S. Chung, L. Y. Jiang, Y. Li and S. Kulprathipanja, *Prog. Polym. Sci.*, 2007, 32, 483-507.
7. T. C. Merkel, H. Lin, X. Wei and R. Baker, *J. Membr. Sci.*, 2010, 359, 126-139.
8. L. M. Robeson, Z. P. Smith, B. D. Freeman and D. R. Paul, *J. Membr. Sci.*, 2014, 453, 71-83.
9. L. M. Robeson, *J. Membr. Sci.*, 2008, 320, 390-400.
10. L. M. Robeson, *J. Membr. Sci.*, 1991, 62, 165-185.
11. H. Vinh-Thang and S. Kaliaguine, *J. Membr. Sci.*, 2014, 452, 271-276.
12. H. Vinh-Thang and S. Kaliaguine, *Chem. Rev.*, 2013, 113, 4980-5028.
13. J. Ploegmakers, S. Japip and K. Nijmeijer, *J. Membr. Sci.*, 2013, 428, 445-453.
14. J. O. Hsieh, K. J. Balkus Jr, J. P. Ferraris and I. H. Musselman, *Micropor. Mesopor. Mater.*, 2014, 196, 165-174.
15. S. Japip, H. Wang, Y. Xiao and T. Shung Chung, *J. Membr. Sci.*, 2014, 467, 162-174.
16. M. Askari and T.-S. Chung, *J. Membr. Sci.*, 2013, 444, 173-183.
17. A. F. Bushell, M. P. Attfield, C. R. Mason, P. M. Budd, Y. Yampolskii, L. Starannikova, A. Rebrov, F. Bazzarelli, P. Bernardo, J. Carolus Jansen, M. Lanč, K. Friess, V. Shantarovich, V. Gustov and V. Isaeva, *J. Membr. Sci.*, 2013, 427, 48-62.
18. N. A. H. M. Nordin, A. F. Ismail, A. Mustafa, R. S. Murali and T. Matsuura, *RSC Advances*, 2014, 4, 52530-52541.
19. B. Zornoza, A. Martinez-Joaristi, P. Serra-Crespo, C. Tellez, J. Coronas, J. Gascon and F. Kapteijn, *Chem. Commun.*, 2011, 47, 9522-9524.
20. B. Seoane, C. Téllez, J. Coronas and C. Staudt, *Sep. Purif. Technol.*, 2013, 111, 72-81.
21. O. G. Nik, X. Y. Chen and S. Kaliaguine, *J. Membr. Sci.*, 2012, 413, 48-61.
22. X. Y. Chen, V.-T. Hoang, D. Rodrigue and S. Kaliaguine, *RSC Advances*, 2013, 3, 24266-24279.
23. X. Y. Chen, H. Vinh-Thang, D. Rodrigue and S. Kaliaguine, *Ind. Eng. Chem. Res.*, 2012, 51, 6895-6906.
24. R. Mahajan and W. J. Koros, *Polym. Eng. Sci.*, 2002, 42, 1420-1431.
25. S. Thomas, I. Pinnau, N. Du and M. D. Guiver, *J. Membr. Sci.*, 2009, 333, 125-131.
26. M. Mulder, *Basic Principles of Membrane Technology*, Kluwer Academic Dordrecht, Second edn., 1996.
27. A. Schneemann, V. Bon, I. Schwedler, I. Senkovska, S. Kaskel and R. A. Fischer, *Chem. Soc. Rev.*, 2014, 43, 6062-6096.
28. E. Stavitski, E. A. Pidko, S. Couck, T. Remy, E. J. M. Hensen, B. M. Weckhuysen, J. Denayer, J. Gascon and F. Kapteijn, *Langmuir*, 2011, 27, 3970-3976.
29. P. Serra-Crespo, E. Gobechiya, E. V. Ramos-Fernandez, J. Juan-Alcañiz, A. Martinez-Joaristi, E. Stavitski, C. E. A. Kirschhock, J. A. Martens, F. Kapteijn and J. Gascon, *Langmuir*, 2012, 28, 12916-12922.
30. K. Tanaka, M. Okano, H. Toshino, H. Kita and K.-I. Okamoto, *J. Polym. Sci., Part B: Polym. Phys.*, 1992, 30, 907-914.
31. C. A. Scholes, C. P. Ribeiro, S. E. Kentish and B. D. Freeman, *J. Membr. Sci.*, 2014, 450, 72-80.
32. D. Hua, Y. K. Ong, Y. Wang, T. Yang and T.-S. Chung, *J. Membr. Sci.*, 2014, 453, 155-167.
33. T.-S. Chung, S. S. Chan, R. Wang, Z. Lu and C. He, *J. Membr. Sci.*, 2003, 211, 91-99.
34. Y. Li, T.-S. Chung, C. Cao and S. Kulprathipanja, *J. Membr. Sci.*, 2005, 260, 45-55.
35. X. Y. Shang, Z. K. Zhu, J. Yin and X. D. Ma, *Chem. Mater.*, 2001, 14, 71-77.
36. Y. Zhang, K. J. Balkus Jr, I. H. Musselman and J. P. Ferraris, *J. Membr. Sci.*, 2008, 325, 28-39.
37. X. Cheng, A. Zhang, K. Hou, M. Liu, Y. Wang, C. Song, G. Zhang and X. Guo, *Dalton Trans.*, 2013, 42, 13698-13705.
38. F. Zhang, X. Zou, X. Gao, S. Fan, F. Sun, H. Ren and G. Zhu, *Adv. Funct. Mater.*, 2012, 22, 3583-3590.
39. J. Liu, F. Zhang, X. Zou, G. Yu, N. Zhao, S. Fan and G. Zhu, *Chem. Commun.*, 2013, 49, 7430-7432.
40. M. Valero, B. Zornoza, C. Téllez and J. Coronas, *Micropor. Mesopor. Mater.*, 2014, 192, 23-28.
41. S. Basu, A. Cano-Odena and I. F. J. Vankelecom, *Sep. Purif. Technol.*, 2011, 81, 31-40.

42. F. Dorosti, M. Omidkhah and R. Abedini, *Chem. Eng. Res. Des.*, 2014, 92, 2439-2448.
43. Y. P. Yampol'skii, I. Pinnau and B. D. Freeman, *Materials science of membranes for gas and vapor separation*, Wiley, Chichester, England, 2006.
44. D. F. Sanders, Z. P. Smith, C. P. Ribeiro Jr, R. Guo, J. E. McGrath, D. R. Paul and B. D. Freeman, *J. Membr. Sci.*, 2012, 409–410, 232-241.
45. R. Guo, D. F. Sanders, Z. P. Smith, B. D. Freeman, D. R. Paul and J. E. McGrath, *Journal of Materials Chemistry A*, 2013, 1, 262-272.
46. M. Mulder, *Basis Principles of Membrane Technology*, Springer Netherlands, London, Second edn., 1996, pp. 226-228.
47. E. V. Perez, K. J. Balkus Jr, J. P. Ferraris and I. H. Musselman, *J. Membr. Sci.*, 2009, 328, 165-173.
48. T. H. Bae, J. S. Lee, W. Qiu, W. J. Koros, C. W. Jones and S. Nair, *Angew. Chem. Int. Ed. Engl.*, 2010, 49, 9863-9866.
49. M. J. C. Ordoñez, K. J. Balkus Jr, J. P. Ferraris and I. H. Musselman, *J. Membr. Sci.*, 2010, 361, 28-37.
50. C. Duan, X. Jie, D. Liu, Y. Cao and Q. Yuan, *J. Membr. Sci.*, 2014, 466, 92-102.
51. T. T. Moore and W. J. Koros, *J. Mol. Struct.*, 2005, 739, 87-98.
52. Y. Li, H.-M. Guan, T.-S. Chung and S. Kulprathipanja, *J. Membr. Sci.*, 2006, 275, 17-28.

Table 1. Designation of copolymers

Copolyimide	x:y ratio	MMM
	2:1	FDH-21
6FDA-$(DAM)_x$-$(HAB)_y$	1:1	FDH-11
	1:2	FDH-12

Table 2. Physical properties of MOFs

Samples	S_{BET} (m^2/g)	S_{meso} (m^2/g)	V_{micro} (cm^3/g)	V_{meso} (cm^3/g)	Bulk density (g/cm^3)
MIL-53	1390	225	0.455	0.275	0.30
NH_2-MIL-53	760	135	0.246	0.115	0.35

Table 3. Density and glass transition temperature (T_g) of homo- and co-polyimides and their MMMs

Membranes	MOF loading (wt.%)		Density (g/cm^3)	T_g (°C)[a]
	MIL-53	NH_2-MIL-53		
FD	-	-	1.347	397
	10	-	1.422	407
	-	10	1.485	408
	-	15	1.513	407
	-	20	1.577	406
FDH-21	-	-	1.355	382
	10	-	1.465	393
	-	10	1.532	401
	-	15	1.574	396
	-	20	1.623	390
FDH-11	-	-	1.361	351
	10	-	1.439	366
	-	10	1.475	372
	-	15	1.531	359
	-	20	1.584	353
FDH-12	-	-	1.368	322
	10	-	1.421	339
	-	10	1.478	341
	-	15	1.522	348
	-	20	1.591	329

[a] Error range is within 5° C

Table 4. CO2 and CH4 permeability, diffusivity, solubility coefficients and their ratios in pure gas measurement at 35 °C and 150 psib

MMMs	MOF loading (wt. %)	P_{CO_2}	P_{CH_4}	D_{CO_2}	D_{CH_4}	S_{CO_2}	S_{CH_4}	P_{CO_2}/P_{CH_4}	D_{CO_2}/D_{CH_4}	S_{CO_2}/S_{CH_4}
FDH-11	-	54.1	3.0	7.3	0.9	74.0	33.3	18.0	8.1	2.2
MIL-53/FDH-11	10	61.4	3.9	8.1	1.1	75.5	34.5	15.7	7.4	2.2
	15	71.1	4.7	9.5	1.3	75.0	35.4	15.1	7.3	2.1
NH_2-MIL-53/FDH-11	10	47.1	0.6	6.7	0.4	70.1	15.0	78.5	16.8	4.7
	15	46.7	0.8	6.1	0.5	77.0	16.0	58.4	12.2	4.8
	20	44.3	1.6	5.3	1.1	83.0	14.6	27.7	4.8	5.1

[b] $P = (10^{-10}$ cm^3(STP) cm^{-1} s^{-1} cmHg^{-1}), $D = (10^{-8}$ cm^2 s^{-1}) and $S = (10^{-3}$ cm^3(STP) cm^{-3} cmHg^{-1})

Table 5 CO_2/CH_4 separation property for selected MOF-based MMMs

MOF	Polymer	Separation measurements	Permeability (Barrer)		CO_2/CH_4 selectivity	Ref.
			CO_2	CH_4		
MOF-5	Matrimid®	2 atm, 35° C	20.2	0.45	44.9	[47]
ZIF-90	Matrimid®	2 atm, 25° C	10	-	36	[48]
ZIF-90	6FDA-DAM	2 atm, 25° C	590-720	-	34-37	[48]
ZIF-8	Matrimid®	2.6 atm, 35° C	9	0.1	90	[49]
ZIF-8	PIM-1	1 atm, 20-22° C	6300	430	14.7	[17]
$Cu_3(BTC)_2$	Matrimid®	2 atm, 35° C	24.8	-	37.8	[50]
$Cu_3(BTC)_2$	ODPA-TMPDA	2 atm, 35° C	160	-	28	[50]

Figure Captions

Fig. 1. Structure of copolyimide precursor FDH.

Fig. 2. SEM images of (A) NH2- MIL-53 and (B) MIL-53.

Fig. 3. Particle size distributions determined from a suspension in ethanol and acidic buffer of MIL-53 and NH2-MIL-53, respectively, using DLS analysis

Fig. 4. FTIR spectra of NH2-MIL-53 and MIL-53.

Fig. 5. FTIR spectra between 3200 and 3800 for NH2-MIL-53 and the corresponding MMMs

Fig. 6. XRD patterns of (A) neat FDH-11; (B) 10 wt%; (C) 15wt% NH2-MIL 53/FDH-11 MMMs and (D) neat NH2-MIL-53.

Fig. 7. XRD patterns of (A) 15 wt% MIL-53/FDH-11 and (B) neat MIL-53.

Fig. 8. SEM micrographs of hydroxyl-copolyimide FDH-11 based MMMs as illustration for particle distribution at loadings of (A) 10 wt%, (B) 15 wt% and (C) 20 wt% NH2-MIL-53

Fig. 9. Illustration for particle agglomeration in a non-hydroxyl polyimide-based MMM containing 10 wt% NH2-MIL-53.

Fig. 10. SEM micrographs of (A) 10 wt% and (B) 15 wt% MIL-53/FDH-11 MMMs.

Fig. 11. (A) CO2 permeability and (B) CO2/CH4 separation factor of the MMMs based on FD and three FDH copolyimides filled with NH2-MIL-53 as a function of MOF loading, in gas mixture of CO2:CH4 = (50:50) at 35°C and 150 psi.

Fig. 12. (A) CO2 permeability and (B) CO2/CH4 separation factor of the MMMs based on FD and three FDH copolyimides filled with MIL-53 as a function of MOF loading, in gas mixture of CO2:CH4 = (50:50) at 35°C and 150 psi.

Fig. 13. CO2/CH4 separation performance of homo-, co-polyimides and their MMMs filled with NH2-MIL-53.

Fig. 14. CO2/CH4 separation performance of homo-, co-polyimides and their MMMs filled with MIL-53.

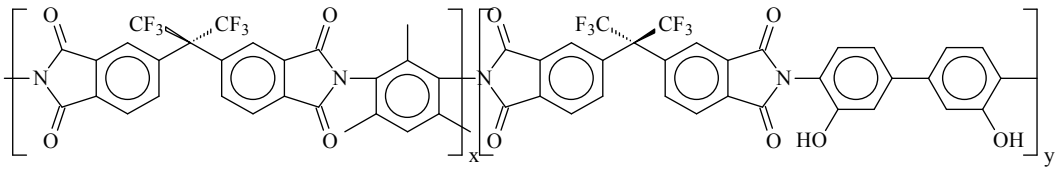

Fig. 1. Structure of copolyimide precursor FDH.

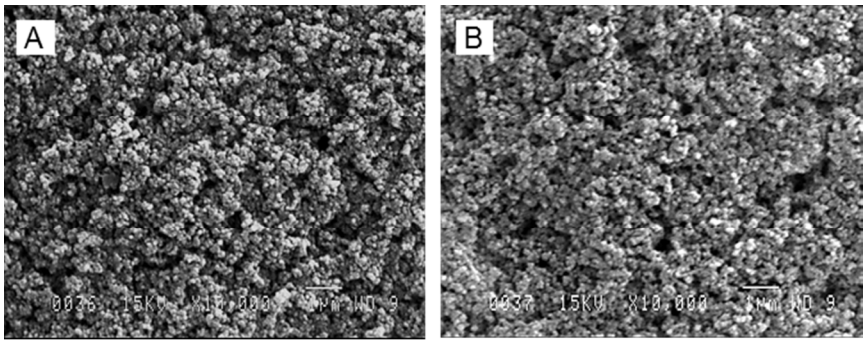

Fig. 2. SEM images of (A) NH_2- MIL-53 and (B) MIL-53.

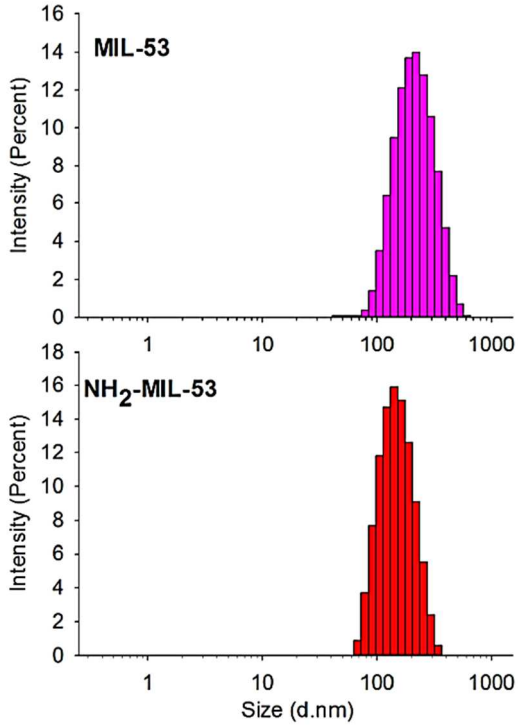

Fig. 3. Particle size distributions determined from a suspension in ethanol and acidic buffer of MIL-53 and NH_2-MIL-53, respectively, using DLS analysis

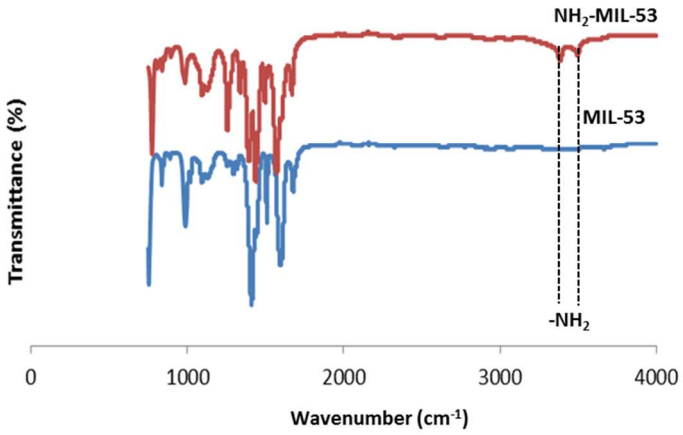

Fig. 4. FTIR spectra of NH_2-MIL-53 and MIL-53.

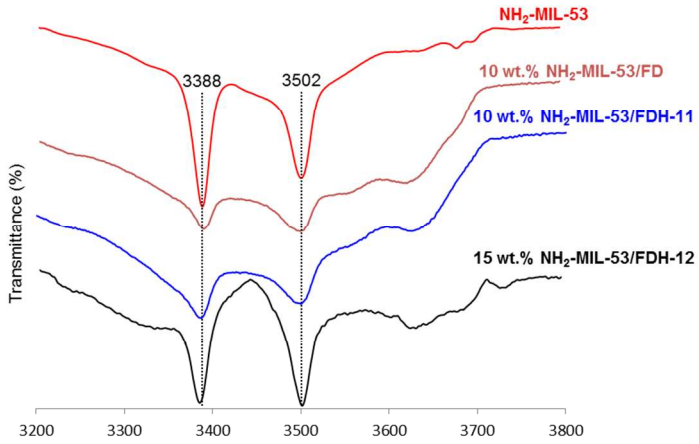

Fig. 5. FTIR spectra between 3200 and 3800 for NH_2-MIL-53 and the corresponding MMMs

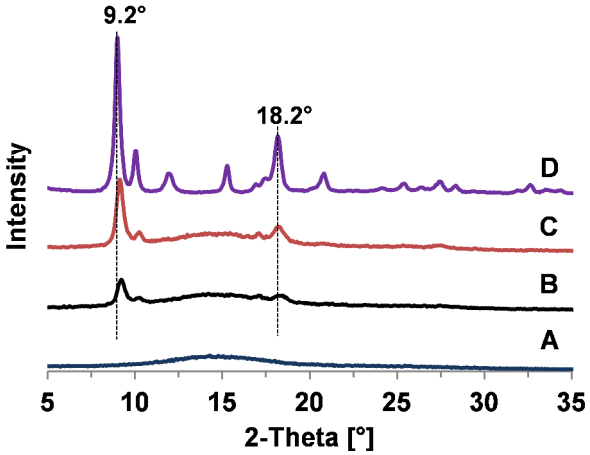

Fig. 6. XRD patterns of (A) neat FDH-11; (B) 10 wt%; (C) 15wt% NH_2-MIL 53/FDH-11 MMMs and (D) neat NH_2-MIL-53.

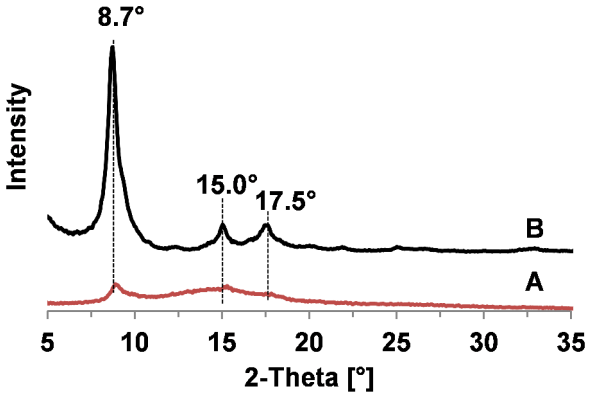

Fig. 7. XRD patterns of (A) 15 wt% MIL-53/FDH-11 and (B) neat MIL-53.

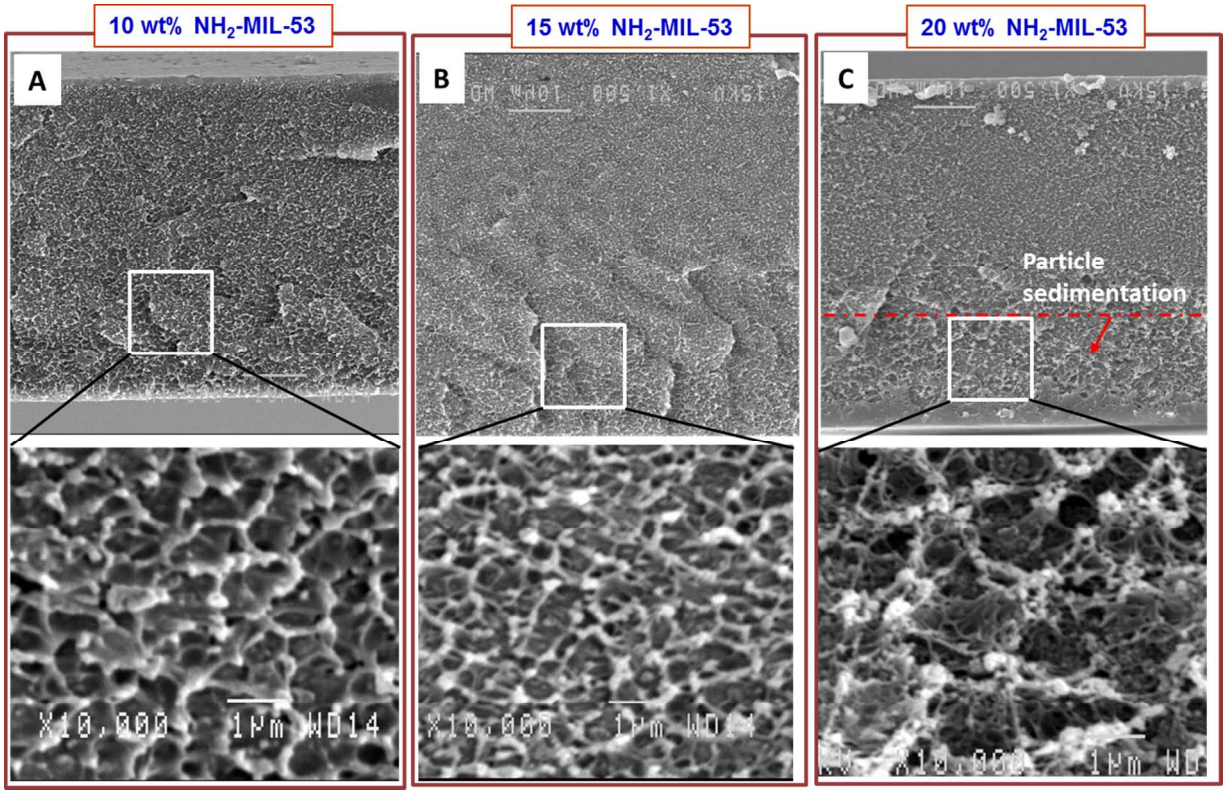

Fig. 8. SEM micrographs of hydroxyl-copolyimide FDH-11 based MMMs as illustration for particle distribution at loadings of (A) 10 wt%, (B) 15 wt% and (C) 20 wt% NH_2-MIL-53

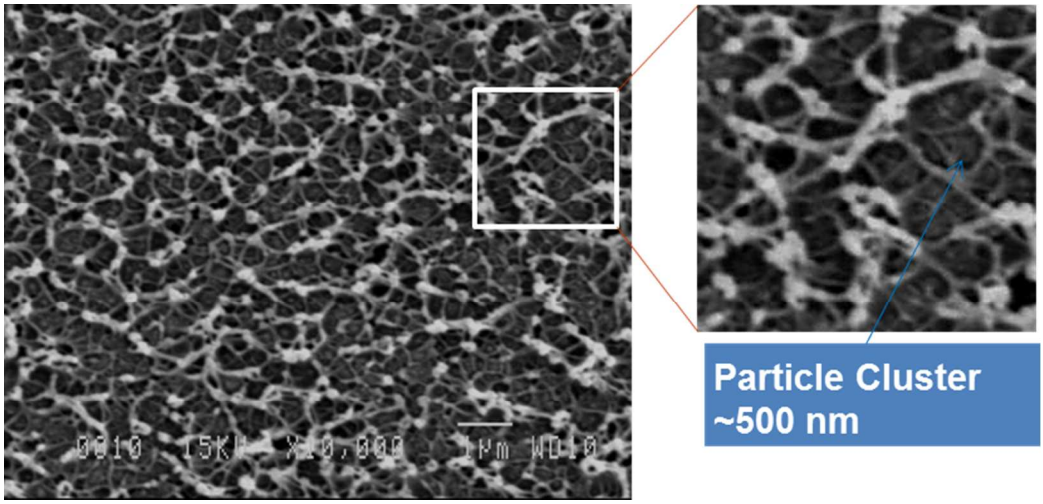

Fig. 9. Illustration for particle agglomeration in a non-hydroxyl polyimide-based MMM containing 10 wt% NH_2-MIL-53.

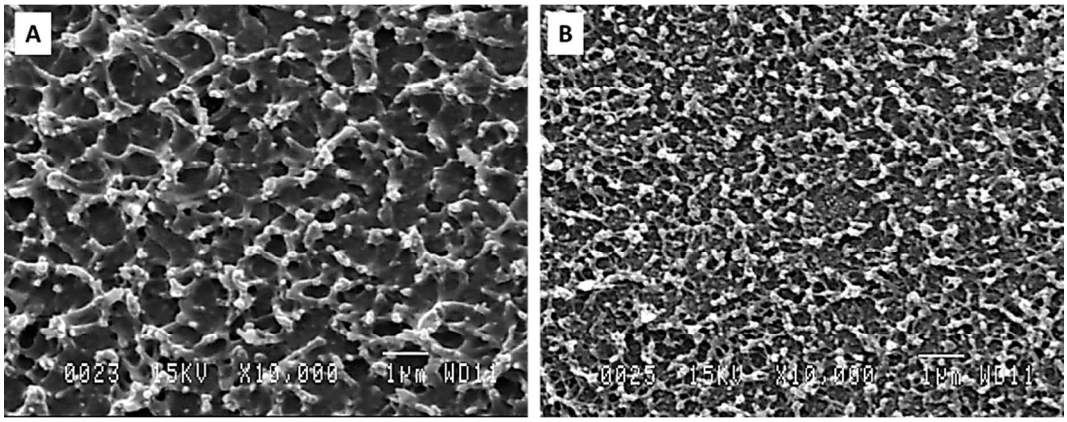

Fig. 10. SEM micrographs of (A) 10 wt% and (B) 15 wt% MIL-53/FDH-11 MMMs.

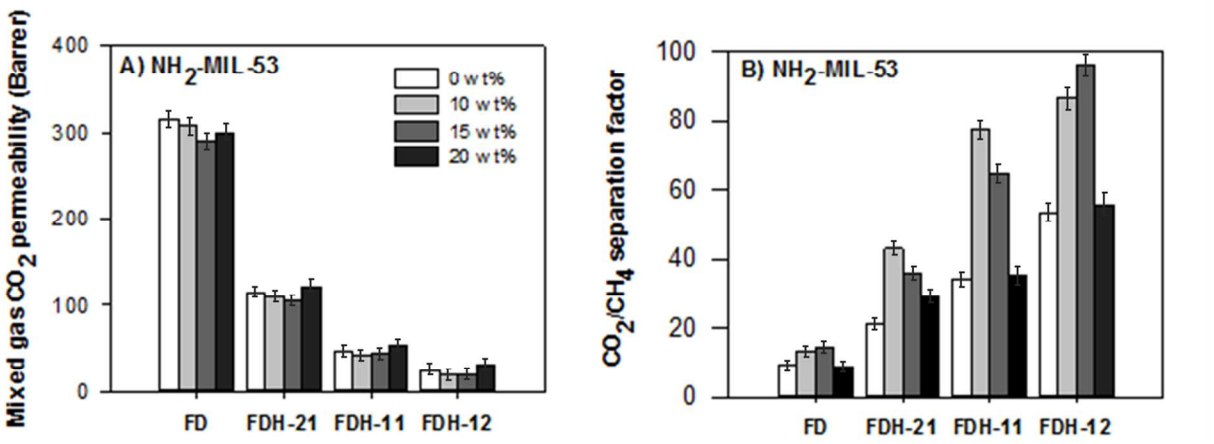

Fig. 11. (A) CO2 permeability and (B) CO_2/CH_4 separation factor of the MMMs based on FD and three FDH copolyimides filled with NH_2-MIL-53 as a function of MOF loading, in gas mixture of CO_2:CH_4 = (50:50) at 35°C and 150 psi.

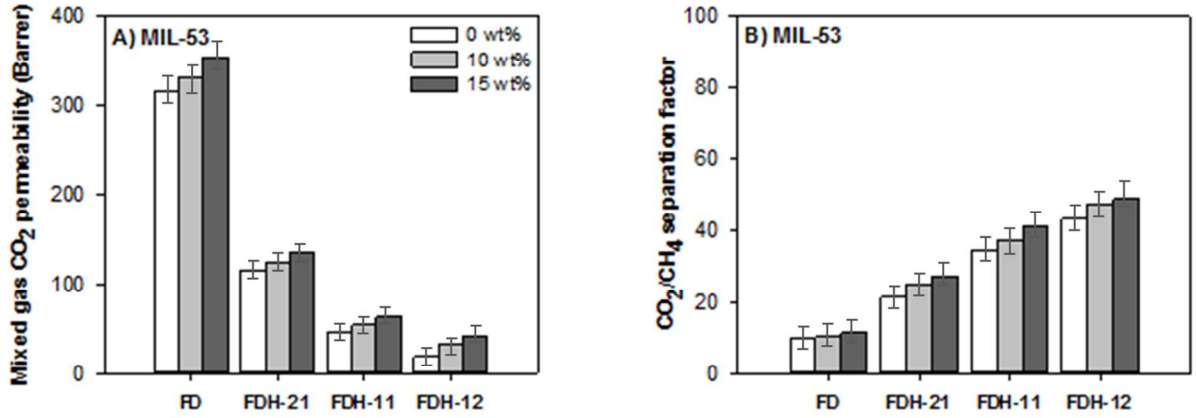

Fig. 12. (A) CO2 permeability and (B) CO_2/CH_4 separation factor of the MMMs based on FD and three FDH copolyimides filled with MIL-53 as a function of MOF loading, in gas mixture of CO_2:CH_4 = (50:50) at 35°C and 150 psi.

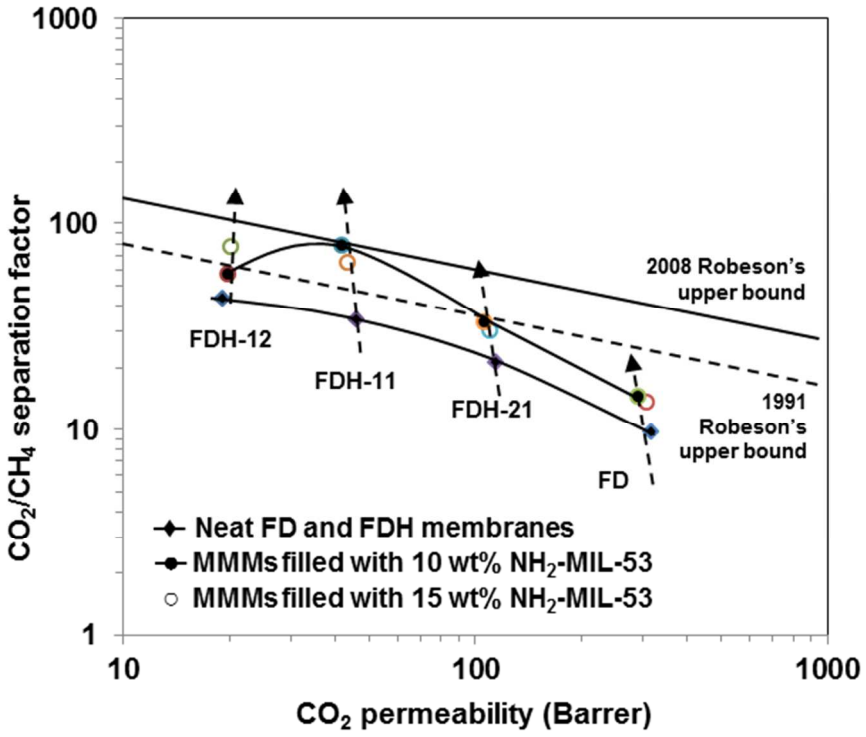

Fig. 13. CO_2/CH_4 separation performance of homo-, co-polyimides and their MMMs filled with NH_2-MIL-53.

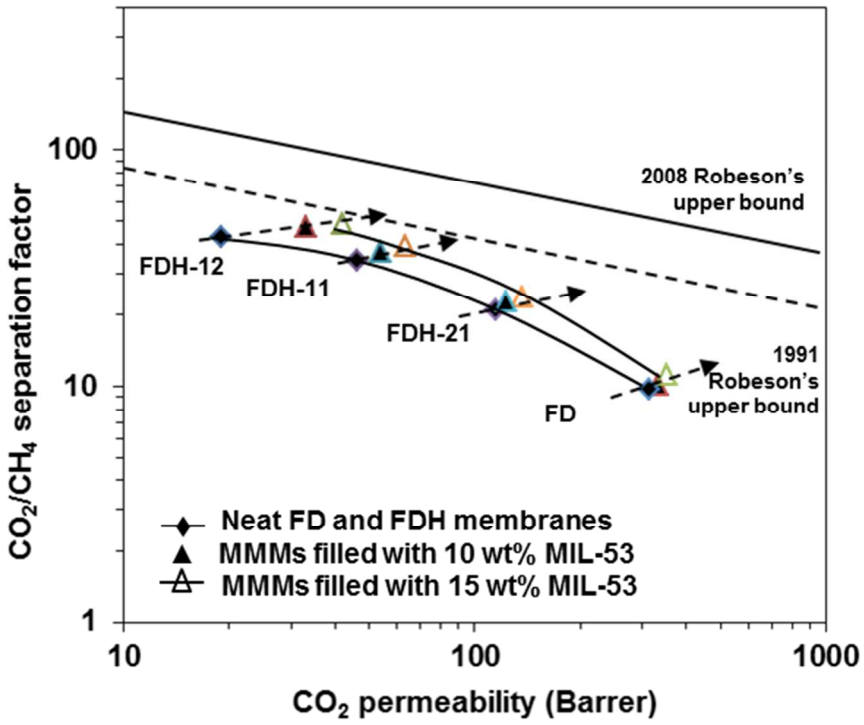

Fig. 14. CO_2/CH_4 separation performance of homo-, co-polyimides and their MMMs filled with MIL-53.